Numerical Analysis of Damage Mechanism on Low-velocity Impact of GLARE 5 Fiber-metal Laminates

YUN WAN *, GUSHENG TONG, SHENSHEN CHEN AND YONGHU HUANG

[a]*School of Civil Engineer and Architecture, East China Jiaotong University, Nanchang, China*

ABSTRACT

The impact performance play an important role in marine material. A numerical methodology including user material subroutine VUMAT, Johnson–Cook flow stress model and surface-based cohesive behavior is carried out to simulate the damage evolution of the impact of GLARE 5 fiber-metal laminates (FML). Specially, user material subroutine VUMAT and surface-based cohesive behavior are employed to solve composite and interface delamination in numerical simulation of low-velocity impact on GLARE 5 FML. By parameters study, proper properties of fiber reinforced layers and surface-based cohesive behavior are given. Moreover, the damage progression of fiber reinforced layers, aluminum alloy layers and delamination in FML are analyzed, respectively. The low-velocity damage mechanism of GLARE 5 is investigated by combining histories of absorbed energy, deflection, contact force and damage evolution. After comparing and analyzing three kinds of damage evolution and the curves of history of absorbing energy, central deflection and contact force, our simulations show that aluminum alloy layers play an important role in improving the performance of low-velocity impact for composites material.

KEYWORDS: *Low-velocity impact, GLARE 5, VUMAT, Surface-based cohesive Behaviour, Damage evolution*

1. INTRODUCTION

Fiber metal laminates (FMLs) are hybrid structures consisting of metal sheets and fiber reinforced plastic layers. The name GLARE reflects the combination of aluminum alloy layers and glass fiber reinforced layers was first developed at Delft University[1–4]. The outside layers of fiber–metal laminate are always metal

J. Polym. Mater. Vol. **34,** No. 3, 2017, 539-552

Correspondence author e-mail: wanyun0505@163.com

and shield the fiber reinforced layers from moisture penetration and scratching. Aluminum sheets with thickness of 0.3–0.4 mm were proven to be optimum while the thickness of the fiber-reinforced layer may vary [5]. FMLs are designed to be a good damage-tolerant material (incl. slow crack propagation) due to fatigue in aerospace structures. For example, high fatigue resistance is achieved by fiber bridging of fatigue cracks [6,7]. If a crack has initiated in the aluminum alloy layers, some limited delamination will occur at the interfaces between the metal and the fibers. That will accommodate stress re-distribution from the metal to unbroken fibres in the wake of crack. Crack bridging provided by the strong fiber restrains crack opening, and thus reduces the driving force for crack growth in the metal layers [8] .GLARE is utilised in the aircraft upper fuselage and the leading edge surfaces of the vertical and horizontal tail planes in the Airbus™ A380 [9]. Impact damage is an important type of failure in aircraft structures. Among different types of damages in an aircraft such as fatigue, corrosion and accidental (impact) damage, and associated repairs. As Volt [10] reported impact damage is usually located around the doors, on the nose of the aircraft, in the cargo compartments and at the tail (due to tail scrape over the runway). Impact damage of aircraft is caused by sources such as: runway debris (in order of 60 m/s), hail (on the ground 25-60 m/s and in flight in the order of hundreds of meter per second), maintenance damage or dropped tool (less than 10 m/s), bird strike (high velocities), ice from propellers striking the fuselage, engine debris, tire shrapnel from tread separation and tire rupture and ballistic impact (for military aircraft).

In general, the FML analysis by means of computer-aided engineering software offers a substantial reduction of costs in comparison with experimentation which makes it highly attractive for practicing engineers. By using the commercial finite element codes ABAQUS, low velocity impact problems on FMLs was simulated by Song *et al.* [11]. Compared the experiment results with numerical results in impact load-time histories and energy-time histories. The load-time history, maximum deflection, and damage progression caused by impact loading were examined by Seo H *et al.* [12] and Sadighi *et al.* [13] used ABAQUS to study low-velocity impact of GLARE 5/3 laminates. They concluded that for low velocity impact, the shape of elements is more important than the type of failure criteria. Low-velocity impact loading on FMLs was modeled by Fan *et al.* and *Asaee et al.* [14,15] using ABAQUS/explicit. Cross-sections of the perforated FMLs were predicted and compared with experimental data. LS-DYNA is employed by Tian *et al.* [16] to simulate the materials performance gradual degradation.

However, according to the observation reported in [17-19] severe damage around the impact site was induced by small indenters during drop-weight impact on GLARE 2 and 3 and energy dissipated through local damage (fracture, delamination and plastic dent). Besides, delamination could reduce the strength of FMLs. So, it should not be ignored. Guan *et al.* [20] conducted ABAQUS/Explicit code with cohesive element to simulate the delamination of low-impulse blast behavior of fiber-metal laminates. Besides, Guan *et al.* [21] presented experimental and simulative structural behavior of fiber metal laminates subjected to a low

velocity impact without delamination and cohesive elements. By using finite element software LS-DYNA with implemented material model MAT162 based on damage mechanics theory and the damaged zone shape, the delaminated area of composite laminates with low velocity impact is discussed in L. Maio *et al.*' [22] simulation.

In the present study, User material subroutine VUMAT, Johnson–Cook flow stress model, and surface-based cohesive behavior are employed to create a numerical methodology investigation on the impact response of GLARE 5 (2/1) composite materials. Not only histories of absorbed energy, central displacement, and the contact force for GLARE 5 with (2/1) could be shown in our numerical simulations, but the material damage evolution and interface delamination of GLARE 5, which is hardly to get through the experimental method, are also presented. The whole damage process of low-velocity impact on GLARE 5 FML is presented in our simulations.

2. EXPERIMENTAL

2. Materials and geometry models for low-velocity impact response

As shown in A. Seyed Yaghoubi *et al.'* [23] experiments, all GLARE panels considered in this study consist of 2024-T3 aluminum alloy with a thickness of 0.305 mm per layer and S2-glass-epoxy layer, each with a thickness of 0.508 mm. Each S2-glass-epoxy layer has a layup orientation of [0°/90°]s. GLARE 5 panels with various thicknesses were cut into square specimens with dimensions of 101.6 × 101.6 mm.

Impact response and damage pattern of GLARE 5 subjected to low-velocity impact with various impact energy levels were investigated using C-scan, optical pictures, and mechanical cross-sectioning techniques at room temperature. All impact tests were conducted using an Instron Dynatup 8250 pneumatic-assisted, instrumented drop-weight impact tester. The specimens were clamped circumferentially along a diameter of 76.2 mm (3 in.) in the specimen fixture and impacted by a hemispherical steel impactor of diameter 16 mm with 12.91 kg. A pair of pneumatic brakes was also used to ensure there were no multiple strikes during impact test. Histories of absorbed energy, central displacement, contact force, and force-deflection for GLARE 5 with different configuration are shown in A. Seyed Yaghoubi *et al.*' [23] experiments. Moreover, the C-scan results show the entire damage contour under 30J impact energies using the 12.9kg impactor mass.

3. Finite element model of low-velocity impact response

3.1. Finite element model and element type

The finite element computer software ABAQUS/Explicit was used to develop numerical simulations of the FML panels subjected to low-velocity impact. The finite element model of the impact system with the details of a typical FML lay-up is illustrated in Fig. 1. The spherical shaped impactor is defined as a rigid body with radius of 8mm. To save computational time, the coarser mesh was employed in the out area element, besides, the impactor was placed just on top of the sandwich panel and an initial velocity was specified. In addition, critical regions in the impact area was packed with more elements in order to capture the results with some accuracy. The type of all elements is C3D8R.

3.2. Damage modes and material properties

Aluminum alloy and glass–fibre laminate have different mechanical properties, different constitutive relations were used to model their respective mechanical behavior. The Johnson-Cook flow stress model was used for aluminum alloy [24]. The details of the material properties and parameters for Johnson-Cook flow stress model are shown in Table 1.

Meanwhile, for glass fiber reinforced layers, the Hashin damage criteria which were developed in 1980. VUMAT is used to define the mechanical constitutive behavior of material. In this investigation, 3D Hashin failure criteria were used [27]. Six different failure modes (matrix tensile and compression, fiber tensile and compression failure). When matrix/fiber tensile or

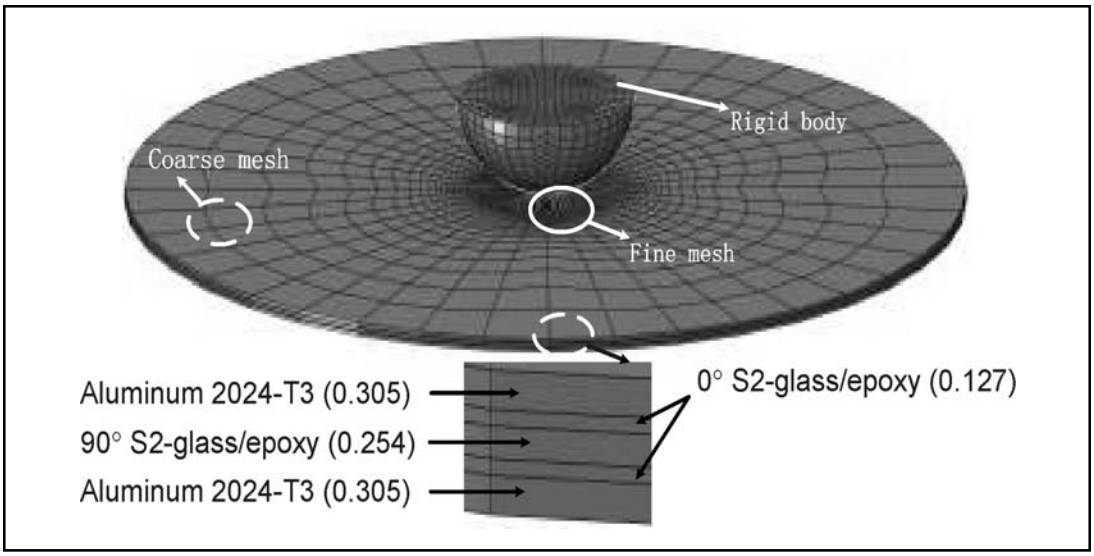

Fig. 1. Finite element model for the impact analysis of FML

TABLE 1. Material properties of aluminium alloy [25, 26]

Elastic parameters	E=72GPa, μ=0.33
Yield surface parameters	A=359 Mpa, B=455 Mpa, C=0.15, m=1, n=0.34
Failure parameters	d_1=0.13, d_2 =0.13, d_3=1.5, d_4=0.011
Fracture energy	GI_C=8 kJ/m_2

compressive failure occurs in a ply, then the material properties in that ply are degraded. As shown in Table 2, Tan's [28] method was used with a corrected factor 'a' in this paper. Meanwhile, the degradation criteria flow chart of the finite element analysis (FEA) with VUMAT is shown in Fig. 2. Material properties of UD S2 glass/FM 94 epoxy prepreg layers is shown in Table 3.

At the interface between the aluminium alloy and the fibre reinforce layer. Surface-based cohesive behavior (SCBC) was employed to simulate the crack propagation. SCBC provides a simplified way of modeling cohesive connections with negligibly small interface thicknesses using the traction-separation constitutive model.

The formulae and laws that govern surface-based cohesion are very similar to those used for cohesive elements with traction-separation behavior: linear elastic traction-separation, damage initiation criteria, and damage evolution laws. The initial response is assumed to be linear. If the damage initiation criterion is specified without a corresponding damage evolution model, ABAQUS evaluates the damage initiation criterion for output purposes only; there is no effect on the response of the cohesive surfaces (i.e., no damage will occur). Cohesive surfaces do not undergo damage under pure compression [30].

Damage initiation criteria

Maximum separation criterion was employed in our simulations, this criterion can be represented as

$$MAX\left\{\frac{\langle\delta_n\rangle}{\delta_n^{\max}},\frac{\delta_s}{\delta_s^{\max}},\frac{\delta_t}{\delta_t^{\max}}\right\}=1 \qquad (9)$$

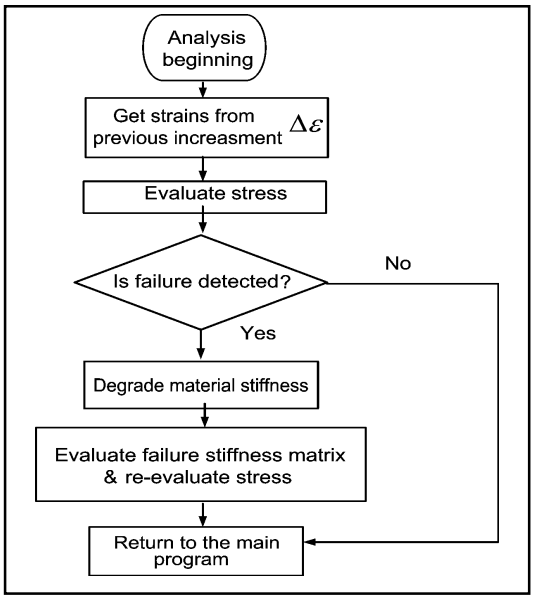

Fig. 2. The flow chart of VMAT

TABLE 2. Material property degradation criteria

Failure mode	Tan 's[28] Degradation criteria	Our Degradation criteria
Delamination ($\sigma_{33} > 0$)	$Q_d = 0.2Q$ ($Q = E_{33}, G_{31}, G_{23}, \nu 31, \nu_{23}$)	$Q_d = a*0.2Q$ ($Q = E_{33}, G_{31}, G_{23}, \nu_{31}, \nu_{23}$)
Delamination ($\sigma_{33} < 0$)	$Q_d = 0.2Q$ ($Q = E_{33}, G_{31}, G_{23}, \nu_{31}, \nu_{23}$)	$Q_d = a*0.2Q$ ($Q = E_{33}, G_{31}, G_{23}, \nu_{31}, \nu_{23}$)
Matrix tensile	$Q_d = 0.2Q$ ($Q = E_{22}, G_{12}, G_{23}, \nu_{12}, \nu_{23}$)	$Q_d = a*0.2Q$ ($Q = E_{22}, G_{12}, G_{23}, \nu_{12}, \nu_{23}$)
Matrix compression	$Q_d = 0.2Q$ ($Q = E_{22}, G_{12}, G_{23}, \nu_{12}, \nu_{23}$)	$Q_d = a*0.4Q$ ($Q = E_{22}, G_{12}, G_{23}, \nu_{12}, \nu_{23}$)
Fiber tensile	$Q_d = 0.07Q$ ($Q = E_{11}, G_{12}, G_{31}, \nu_{12}, \nu_{31}$)	$Q_d = a*0.07Q$ ($Q = E_{11}, G_{12}, G_{31}, \nu_{12}, \nu_{31}$)
Fiber compression	$Q_d = 0.07Q$ ($Q = E_{11}, G_{12}, G_{31}, \nu_{12}, \nu_{31}$)	$Q_d = a*0.07Q$ ($Q = E_{11}, G_{12}, G_{31}, \nu_{12}, \nu_{31}$)

Note: Q and Q_d stand for initial stiffness and failure stiffness, respectively.

TABLE 3. Material properties of UD S2 glass/FM 94 epoxy prepreg layers [23, 29]

Property	Value	Property	Value
E_{11}(GPa)	54	X_T (Mpa)	1900
E_{22}(GPa)	9.4	X_C (Mpa)	520
E_{33}(GPa)	9.4	Y_T (MPa)	57
$\mu 12$	0.0575	Y_C (MPa)	285
$\mu 13$	0.0575	Z_T (MPa)	57
$\mu 23$	0.33	Z_C (MPa)	285
G_{12}(GPa)	5.6	S_{12} (GPa)	76
G_{13}(GPa)	5.6	S_{13} (GPa)	76
G_{23}(GPa)	5.6	S_{23} (GPa)	76

.

Damage initiation evolution: a scalar damage variable, D, represents the overall damage at the contact point. It initially has a value of 0. If damage evolution is modeled, D monotonically evolves from 0 to 1 upon further loading after the initiation of damage. The contact stress components are affected by the damage according to

$$t_n = \begin{cases} (1-D)\,\bar{t}_n, \ \bar{t}_n \geq 0 \\ \bar{t}_n \quad \text{otherwise (no damage to compressive stiffness)} \end{cases} \tag{10}$$

$$t_s = (1-D)\,\bar{t}_s, \tag{11}$$

$$t_t = (1-D)\,\bar{t}_t, \tag{12}$$

where $\bar{t}_n$, $\bar{t}_s$ and $\bar{t}_t$ are the contact stress components predicted by elastic traction-separation behavior for the current separations without damage.There are evolution based on effective separation and energy in surface-based cohesive behavior. Here, power law form energy evolution was employed in our simulation. It is given by

$$\left\{\frac{G_n}{G_n^C}\right\}^\alpha + \left\{\frac{G_s}{G_s^C}\right\}^\alpha + \left\{\frac{G_t}{G_t^C}\right\}^\alpha = 1 \tag{13}$$

In the expression above the quantities G_n, G_s, and G_t refer to the work done by the traction and its conjugate separation in the normal, the first, and the second shear directions, respectively. G_n^c, G_s^c, G_t^c and refer to the critical fracture energies required to cause failure in the normal, the first, and the second shear directions.

For exponential softening Abaqus uses an evolution of the damage variable, D, that reduces to:

$$D = \int_{\delta_m^0}^{\delta_m^f} \frac{T_{eff}\, d\delta}{G^C - G_0} \tag{14}$$

In the expression above T_{eff} and δ are the effective traction and separation, respectively. G_0 is the elastic energy at damage initiation. In this case the traction might not drop immediately after damage initiation. A summary of cohesive element material properties and references is given in Table 4 [31] and parameters study is implemented on the critical fracture energies at following section.

TABLE 4. Based-cohesive behaviour properties

Property	Value	Property	Value	Property	Value
K_n(N/mm$_3$)	2E6	δ_n^{max}(mm)	2.5E-5	G_n^c (N/mm)	parameters study
K_s(N/mm$_3$)	0.75E6	δ_s^{max}(mm)	6.65E-5	G_s^c(N/mm)	parameters study
K_t(N/mm$_3$)	0.75E6	δ_t^{max}(mm)	6.65E-5	G^c_t (N/mm)	parameters study

4. RESULTS AND DISCUSSIONS

4.1. Parameters study of fibre reinforced layers stiffness degradation and damage evolution fracture energy.

According to Hashin damage criteria and Tan's [28] progressive failure model, the stiffness is degenerated when the related failure occurred. But the degree of Tan's [28] stiffness degradation is not proper for our simulation totally. As shown in Table 2, degradation criteria coefficient 'a' which is based on Tan' degradation criteria is employed in our simulation. With different degradation coefficient, different impact responses of GLARE 5 (2/1) are observed under impact energy of 30 J. By comparing the histories of absorbed energy, central displacement, contact force between simulate and experimental results, proper degradation criteria coefficient in our simulation model is found.

In Fig. 3a-3c, curves of histories of absorbed energy, central displacement and contact force versus time for GLARE 5 with (2/1) are shown, respectively. As can be seen in Fig. 3a & 3b, obvious rebound phenomenon happened when

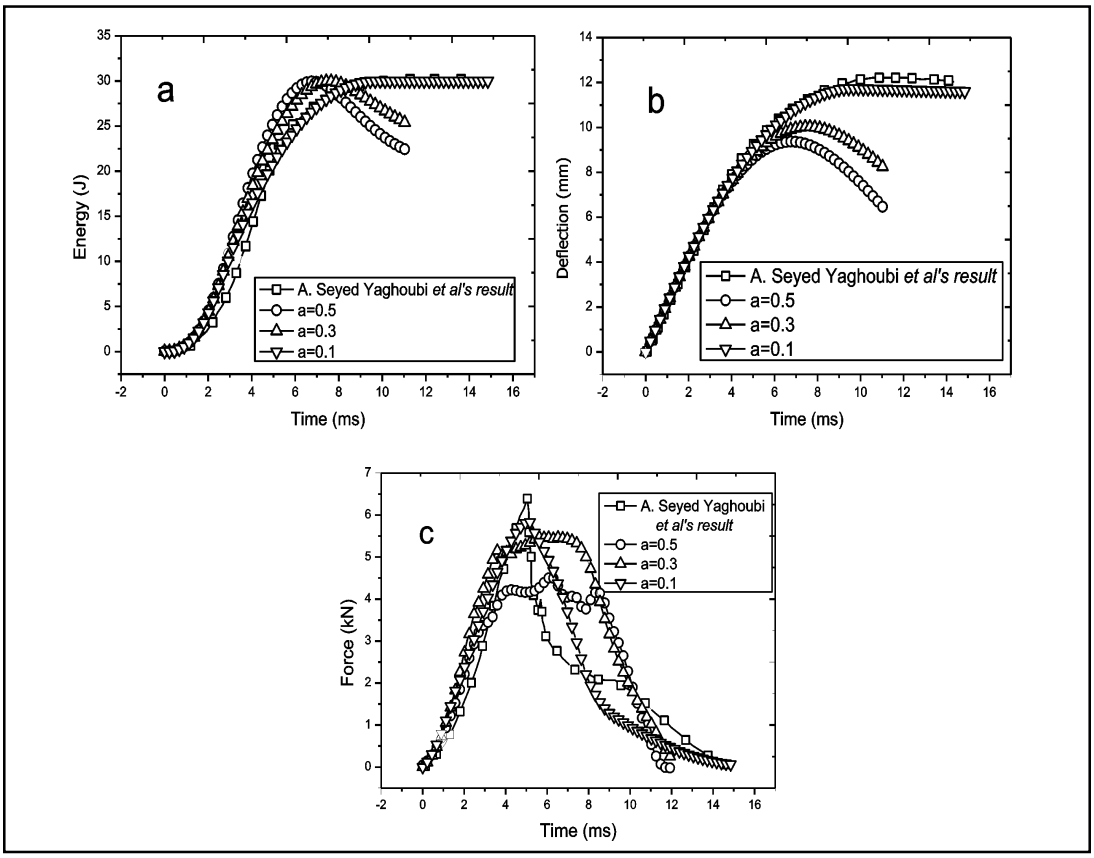

Fig. 3. Impact responses of GLARE 5 (2/1 under 30 J impact energy)

a=0.5 or a=0.3. However, when 'a' comes to 0.1, no rebound occurred as the GLARE 5 (2/1) panel absorbed all kinetic energy. The finial deflection of the centre point is 11.73 mm and the contact force reached peak value of 5.85 kN at 5.1 ms. When a=0.1, the results are in great agreement with the experiment results. So, a=0.1 is proper for the simulation model.

Parameters are shown in Table 4. To investigate the effect of damage evolution fracture energy

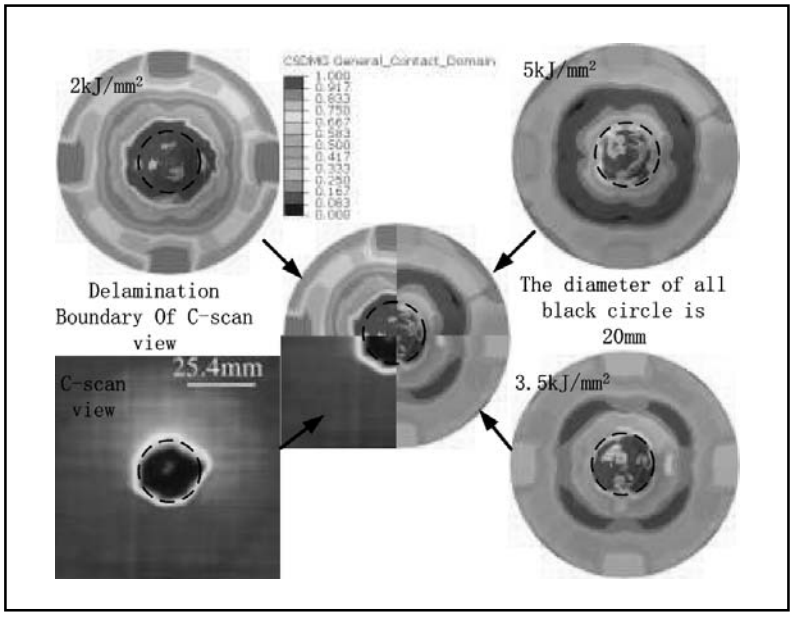

Fig. 4. Comparing damage area between experiment result (the C-scan backside view) and Damage variable for cohesive surfaces in general contact (CSDMG) D of backside aluminium alloy and glass–fibre laminate interface when the fracture energies $G_n^c = G_s^c = G_t^c$ =2, 3.5, and 5 *kJ/mm²* respectively

of surface-based cohesive behavior, we calibrate the intrinsic critical fracture energy $G_n^c = G_s^c = G_t^c$ =2, 3.5, and 5 kJ/mm², respectively. Fig. 4 shows comparison of damage area between experiment result (the C-scan backside view) and simulated results for the interface delamination between the backside aluminum alloy and glass–fiber laminate, where the damage variable for cohesive surfaces in general contact the overall (Damage variable for cohesive surfaces in general contact (CSDMG)) is the parameter 'D' in Equation 14. The area of the entire damage in S-can view can be considered as the delaminated area. The influence of critical fracture energy on CSDMG can be seen. When $G_n^c = G_s^c = G_t^c$ = 5 kJ/mm² the delamination area of simulated is much smaller than backside C-scan result, however, when G_n^c, G_s^c, and G_t^c come to 2 kJ/mm², the delamination region is much bigger. The simulation results is in better agreement with the experiment results very well when $G_n^c = G_s^c = G_t^c$ =3.5 kJ/mm².

4.2. The damage history of GLARE 5 (2/1) fibre reinforced layers. Not only the absorbed energy, central displacement, and contact force are simulated, but the damage history of the fiber reinforced layers is got as well. According to Hashin criteria, there are six failure modes. In the low-velocity impact on GLARE 5, fiber tensile is the dominated failure mode, so the history of the fiber tensile failure should be paid more attention on. Fig. 5 shows the history of

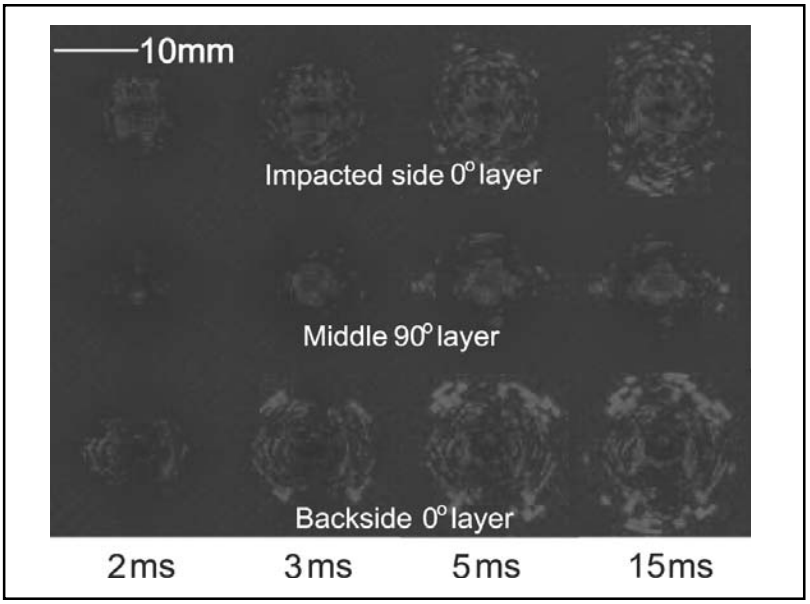

Fig. 5. The history of fibre tensile damage (in order to getting accurate element location, deformation scale factor is set deformation scale factor as 0.01)

fiber tensile damage (in order to get accurate element location, deformation scale factor fiber tensile damage contour is set as 0.01), which indicates the fiber tensile failure and damage progress under low-velocity impact. The damage of impacted-side, middle, and backside layer of fiber reinforced laminates all initiates from the centre area, then the damage area expands to the out area. For the damage region, the damaged area increases steadily before 5ms, and the growth rate of which decreases after 5 ms. In addition, during the impact history, the backsides layer (0^o) has more damaged elements than the impacted side layer (0^o) and the middle layer(90^o). The middle layer has the fewest fiber damaged elements and the damaged elements concentrate in the centre area. These phenomena indicate that middle fiber reinforced layer is relative safer, while the backside fiber reinforced layer absorbs more kinetic energy of the impactor. Besides, all fibre reinforced layers absorb less energy after 5 ms.

Combining the history of fiber tensile damage in Fig. 5 and the damage evolution of the aluminum alloy layer in Fig. 8, we can find that there is an initiation crack and crack expansion

on the aluminum alloy layer from 4.28 ms to 5 ms, meanwhile, the growth trend of fiber tensile damaged get slow. The deduction could made that when the aluminum alloy layer cracks, the fiber reinforced layers crack along the primary hairline crack of backside aluminum alloy layer, and they absorb less kinetic energy along with a rapidly drop of the contact force as shown in Fig. 3. So the aluminum alloy layer plays a dominated role in the impacted performance of GLARE.

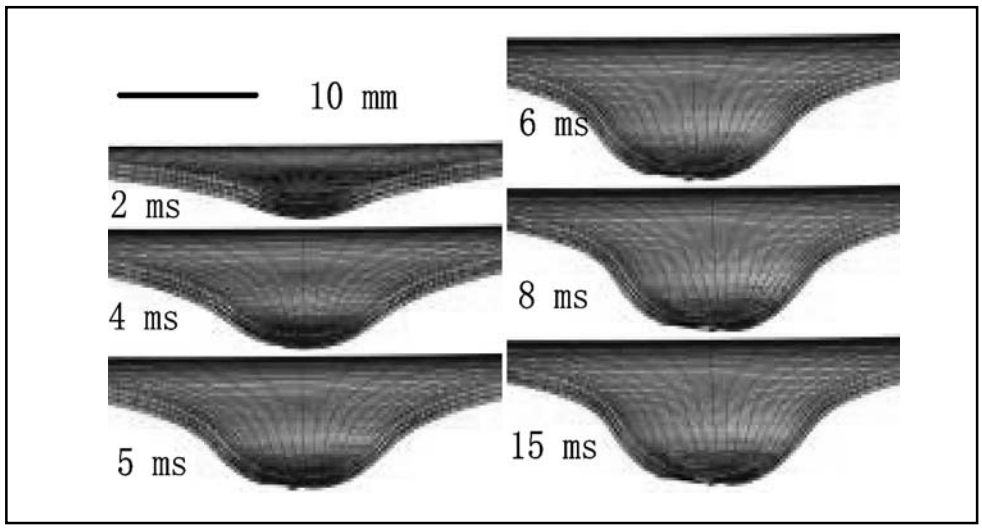

Fig. 6. The history of the deflection

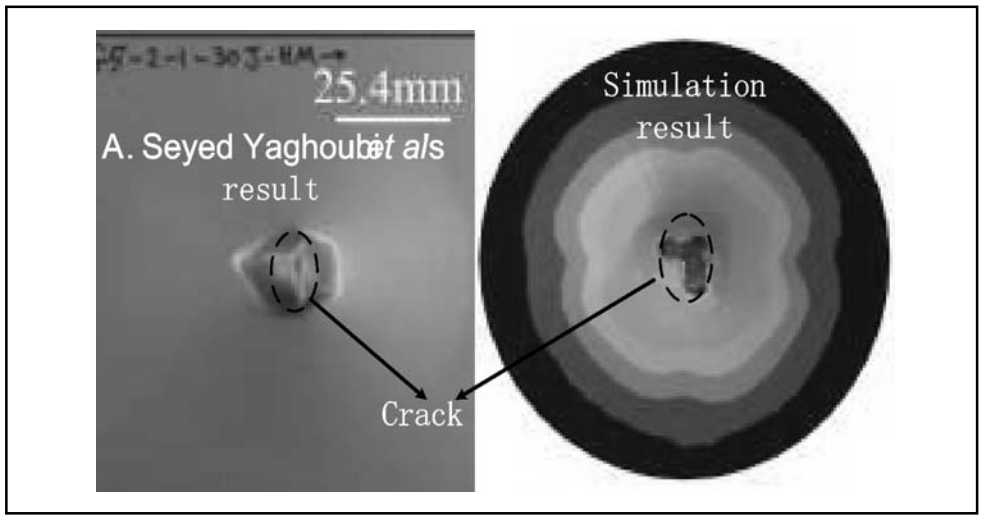

Fig. 7. Comparing backside crack, GLARE 5 (2/1) with 30J, between optical view and simulation result

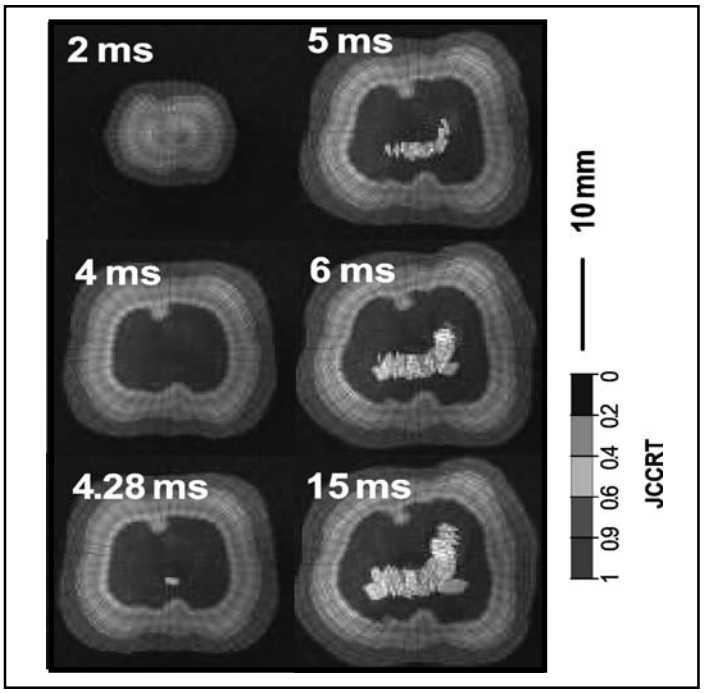

Fig. 8. The Johnson-Cook damage initiation criterion (JCCRT) history of backside aluminium alloy layer

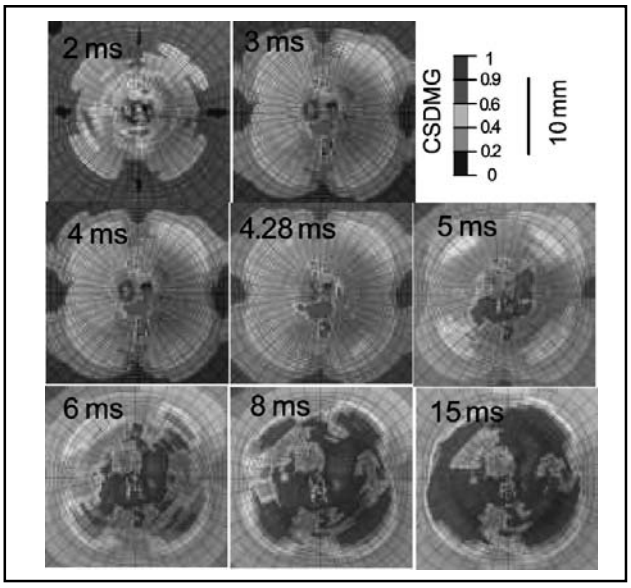

Fig. 9. The CSDMG history of backside interface

4.3. The damage evolution of aluminum alloy layer and interface delamination.

The history of the deflection, the Johnson-Cook damage initiation criterion (JCCRT) history of backside aluminum alloy layer, and CSDMG history of backside interface are shown in Fig.6, Fig.7 and Fig.8, respectively. Fig. 7 shows that the backside aluminum alloy layer's shape and crack length of our simulation agree with A. Seyed Yaghoubi *et al*'s [25] experiment result very well. As shown in Fig. 8, the initial crack of the backside aluminum alloy layer appears at 4.28 ms, and the crack propagation velocity is very high before 5 ms, but then it slows down and the crack makes little change after 6ms. Fig. 9 shows that delamination initiates at 2ms and the delamination region expand very slowly. However, when the time comes to 4.28 ms, just the time when initial crack appears, the delamination region expand along the crack and extend to the surrounding area.

The whole damage process of low-velocity impact on GLARE 5 FML could be summarized as following steps, and it's shown in Table 5.

1. 0ms-4.28ms, damage and deformation of the fibre reinforced layers and aluminum alloy layers evolutes steadily. Meanwhile, a small amount of delamination area appears between fibre reinforced layer and aluminum alloy layer. At 4.28 ms, the absorbed energy and contact force get to 20.4 J and 5.4 kN, respectively.

TABLE 5. The evolution of contact force, absorbed energy, damage of the aluminum layer, damage of composite layer and interface delamination

Time (ms)	Contact force	Absorbed energy	Damage of the aluminum layer	Damage of composite layer	Interface delamination
(0.00,4.28]	↑	↑	↑	↑	→
(4.28,5.00]	↑	↑	↗	↑	↗
(5.00,8.00]	↓	↗	→	↗	↑
(8.00,15.00)	↘	↗	→	↗	↗

2. 4.28ms-5ms, the crack on the aluminum alloy layer extends rapidly, and delamination region expand along the primary hairline crack of backside aluminum alloy layer. The fiber reinforced layers still absorb energy. When the time is 5ms, the absorbed energy is 24.7 J, and the contact force reach the peak value 6.3 kN.
3. After 5ms, the crack propagation velocity of aluminum alloy layer slows down. The crack of aluminum alloy layer is so big that the fiber reinforced layer get damaged and could not absorb energy any more. Meanwhile, the delamination region expand along the crack to the surrounding area and the contact force falls rapidly.

5. CONCLUSION

This work presents a numerical methodology investigation on the impact response of GlARE 5 (2/1) composite materials. The finite element computer software ABAQUS/Explicit is used to develop numerical simulations of GLARE 5 (2/1) FML panels subjected to low-velocity

impact. User material subroutine VUMAT, Johnson–Cook flow stress model, and surface-based cohesive behavior are employed to calculate the damage evolution of fibre reinforced layers, aluminum alloy layers, and interface delamination between fiber reinforced layer and aluminum alloy layer, respectively. Especially, user material subroutine VUMAT and surface-based cohesive behavior are firstly employed to do numerical simulation of low-velocity impact on GLARE 5 FML.

Not only histories of absorbed energy, central displacement, and the contact force for GLARE 5 with (2/1) are shown in our numerical simulations, more meaningfully, the material damage evolution and interface delamination of GLARE 5, which are hardly to obtain by the experimental method, are also presented. The simulation results indicate that backside fiber reinforced layer absorbs most energy and middle layer absorbs least energy. Moreover, aluminum alloy layers dominate the performance of low-velocity impact on GLARE 5 FML.

Acknowledgement

This work is supported by the Primary Research & Development Plan of Jiangxi Province of China (20071BBE50024), The Natural Science Foundation of Jiangxi Province (20171BAB216041) and the National Natural Science Foundation of China (No. 11462005)

REFERENCES

1. A. Volt, *Composites Engineering*, 3 (1993) 911–927.
2. A. Volt, *International Journal of Impact Engineering,* 8 (1996) 291–307.
3. A. Vlot, and M. Krull, *Le Journal de Physique* IV 7.C3 (1997): C3-1045.
4. A. Volt. J.W. Gunnink, In: editor.Norwell: Kluwer Academic Publishers, 2001.
5. A. Volt, and J.W. Gunnink, Netherlands: Kluwer Academic Publishers, (2001): 73-75.
6. R.C. Alderliesten, R. Benedictus, 48th AIAA/ ASME/ASCE/AHS/ASC Structures, Structural Dynamics and Materials Conference; 2007. 23-26 April, Honolo-lulu, Hawai. p. 1-12
7. R.C. Alderliesten, M. Hagenbeek, J.J. Homan, P.A. Hooijmeijer, T.J. De Vries, C.A.J.R. Vermeeren, *Applied Composite Materials,* 10(2003) 223-242.
8. R.C. Alderliesten, R. Benedictus, 48th AIAA/ ASME/ASCE/AHS/ASC Structures, Structural Dynamics and Materials Conference; 2007. 23e 26 April, Honolo-lulu, Hawai. p. 1-12
9. P. Soltani, M. Keikhosravi, R.H. Oskouei, C. Soutis, *Applied Composite Materials,* 18 (2010) 271–282.
10. A. Volt, Rept. LR-718. Delft, The Netherlands: Delft Univ. Of Technology; 1993.
11. S.H. Song, Y.S. Byun, T.W. Ku, W.J Song, J. Kim, B.S. Kang, *Journal Of Materials Science & Technologyt,* 26 (2010) 327-332.
12. H. Seo, J. Hundley, H.T. Hahn, J.M. Yang. *AIAA J.* 48 (2010) 676-687.
13. M. Sadighi, T. Parnanen, R.C. Alderliesten, M. Sayeaftabi, R. Benedictus, *Applied Composite Materials,* 19 (2012) 545-559.
14. J. Fan, Z.W. Guan, W.J. Cantwell, *Composite Structures,* 93 (2011) 2430-2436.
15. Z. Asaee, F. Taheri, *Composite Structures*, 2016, 140: 136-146.
16. S. Tian, Z. Zhou, *Material & Design,* 102 (2016) 142-150.
17. M.R. Abdullah, W.J. Cantwell, *Composites Science and Technology,* 66 (2006) 1682-1693.

18. G. Reyes Villanueva, W.J. Cantwell, *Composites Science and Technology,* 64 (2004) 35-54.

19. Y.X. Liu, B.M. Liaw, SEM X International Congress & Exposition on Experimental and Applied Mechanics Costa Mesa, CA. 2004.

20. T.P. Vo, Z.W. Guan, W.J. Cantwell and G.K. Schleyer, *Composite Structures,* 94 (2012) 954–965.

21. J.Y. Fan, Z.W. Guan and W.J. Cantwell, *Science China Physics, Mechanics and Astronomy* 54.6 (2011): 1168-1177.

22. L. Maio, E. Monaco, F. Ricci and L. Lecce, *Composite Structures,* 103 (2013) 75–85.

23. A. Seyed Yaghoubi, Y. Liu, B. Liaw, *Journal of Aerospace Engineering,* 25 (2012) 409–420.

24. G.R. Johnson, W.H. Cook, In: Proceedings of the seventh international symposium on ballistics; 1983. The Hague, Netherland. pp. 541–547.

25. G. Kay, In: US Department of Energy; 2002

26. D. Lesuer, 1999. U.S. Department of Energy.

27. Z. Hashin, *Journal of Applied Mechanics,* 47 (1980) 329–334

28. S.C. Tan, *Journal of Composite Materials,* 25 (1991) 556-577

29. A. Seyed Yaghoubi, B. Liaw, *Composite Structures,* 94 (2012) 2585–2598.

30. Abaqus 6.9 Documentation. Providence, RI, USA: Dassault Systèmes Simulia Corporation; 2010.

31. Abaqus 6.9 Example Problems Manual 1.4.6. Providence, RI, USA: Dassault Systèmes Simulia Corporation; 2010.

Received: 17-06-2016

Accepted: 31-01-2017